AIAA JOURNAL
Vol. 33, No. 12, December 1995

Viscous Interaction Phenomena in Hypersonic Wedge Flow

Luigi de Luca* and Gennaro Cardone†
University of Naples "Federico II," Naples 80125, Italy
and
Dominique Aymer de la Chevalerie‡ and Alain Fonteneau§
Centre National de la Recherche Scientifique, Poitiers 86036, France

The present paper deals with an experimental investigation carried out to study some aspects of shock/boundary-layer interaction in nominally two-dimensional hypersonic wedge flow, i.e., over flat plate/ramp configurations. These flow conditions are two dimensional only geometrically because some spanwise periodic variations of the heat flux over the ramp in the reattaching flow region are observed. The measurements, basically made by means of a computerized infrared (IR) imaging system, have been performed in a blowdown wind tunnel at Mach number equal to 7.14 and unit Reynolds number ranging from 7.6×10^6 to 24×10^6/m. The influence of the leading-edge shape (bluntness and geometry), flat plate length, and ramp angle on the separation region, average heat transfer at reattachment, and wavelength of the heat transfer variations has been analyzed. IR results are compared to other experimental data as well as to semiempirical correlations for the heat flux peak.

Introduction

THE present work deals with a fundamental experimental study of the shock wave/boundary-layer interaction phenomena occurring in the region of deflected control surfaces of hypersonic vehicles and the effect on aerodynamic performance and heating. The objective of this study is to provide a high-quality set of heat transfer data at hypersonic Mach numbers that may contribute to the understanding and modeling of the relevant flow processes and to the design of future hypersonic vehicles.

In order to achieve these objectives, experiments have been carried out to study some cases of shock wave/boundary-layer interaction in two-dimensional hypersonic flow over relatively simple models relative to a flat plate followed by a compression ramp with its hinge line parallel to the model's leading edge. Because of the large variations encountered near the reattachment point, in general the heat flux measurements are difficult to perform. Moreover, although the tested geometrical configurations are nominally two dimensional, some significant three-dimensional effects are to be expected in the reattaching separated (laminar or turbulent) flows. Inger[1] reported an appreciable body of previous papers dealing with vortexlike laterally periodic variations in shear, pressure, and heat transfer that may occur in nominally two-dimensional high-speed reattaching flows. Inger[1] hypothesized that such variations (or oscillations) could be ascribed to the development of Goertler type vortices due to the flow curvature above the separation streamline. Coet[2] carried out surface flow visualizations by means of the oil-film technique, showing some spanwise periodic structures at Mach number 10. Aymer de la Chevalerie and Fonteneau[3] performed other visualizations at Mach 7.14 by means of thermosensitive paints and checked the repeatability of the measurements. Analogous spanwise striations of the heat flux were found by Simeonides[4] at Mach 14 and Aymer de la Chevalerie and Fonteneau[3] at Mach 7.14. From the computational point of view, the Goertler instability in supersonic or hypersonic flows was studied by El-Hady and Verma,[5] Spall and Malik,[6] and Jallade.[7] However, these last papers are concerned with flows over concave walls having a constant streamwise curvature radius. De Luca et al.[8] carried out experimental measurements to validate the numerical findings for concave walls. Rudy et al.[9] simulated the finite span effects in compression-corner flows to obtain a better agreement with the experimental data. As a main result, they found that three-dimensional effects produce a smaller separated-flow region in the centerplane than that predicted in the two-dimensional calculations; however, they did not report any discussion about spanwise periodic variations.

These considerations bring out the need for accurate measurements of the aerodynamic heating in hypersonic compression-corner flows that take into account such three-dimensional characteristics of the viscous interaction. In this paper the effect of parameters, such as unit Reynolds number, leading-edge shape, flat plate length, and ramp angle, has been investigated in a blowdown wind tunnel. The influence on the separation region, average heat transfer at reattachment, heat transfer spanwise variations (over the ramp), and wavelength of periodic oscillations has been determined basically by means of an infrared imaging system (IRIS).

Application of IR thermography to hypersonic wind-tunnel experiments is advantageous because of relatively good spatial resolution, thermal sensitivity, and sufficiently rapid response time that enables it to be used in both thin-skin and thin-film techniques.[10–13] Moreover, the use of an IRIS meets both qualitative and quantitative requirements. The essential features of the thermographic system are that it is nonintrusive, that it allows a complete two-dimensional mapping of the surface to be measured, and that the video signal output may be treated by digital image processing.

Comparisons between IR and thermocouple heat transfer distributions, as well as semiempirical correlations for the heat flux peak, are also presented.

Testing Procedure

Experimental Rig

Experimental tests have been carried out in the hypersonic blowdown tunnel H210 of the Centre d'Etudes Aerodynamiques et Thermiques (CEAT), Poitiers, having a test section diameter of 210 mm. The operating fluid is dry air, which has a typical stagnation temperature of $T_0 = 780$ K (±0.8% uncertainty/nonrepeatability) and a stagnation pressure range of $3\,\text{MPa} < p_0 < 9\,\text{MPa}$ (±0.5% uncertainty/nonrepeatability). Freestream unit Reynolds number Re_u is changed mainly by varying the stagnation pressure and, in the present tests, ranges from 7.6×10^6 to 24×10^6/m (±5% uncertainty/nonrepeatability). A properly designed nozzle has been employed so as to obtain a nominal freestream Mach number equal to 7.14 (±1.3% uncertainty/nonrepeatability).

Received Feb. 6, 1995; revision received June 12, 1995; accepted for publication June 27, 1995. Copyright © 1995 by the American Institute of Aeronautics and Astronautics, Inc. All rights reserved.

*Associate Professor, Dipartimento di Energetica, Termofluidodinamica, e Condizionamenti Ambientali, P. le Tecchio 80. Member AIAA.
†Research Staff, Dipartimento di Energetica, Termofluidodinamica, e Condizionamenti Ambientali, P. le Tecchio 80.
‡Chargé de Recherche, Laboratoire d'Etudes Aérodynamiques (URA 191), 43 rue de l'Aérodrome.
§Graduate Student, Laboratoire d'Etudes Aérodynamiques (URA 191), 43 rue de l'Aérodrome.

Table 1 Tested models

Model	Ramp angle, deg	Flat plate length, mm	Leading edge	Ramp type	Flat plate type
A	10, 15, 20, 25	40, 90, 125	sharp	solid RTV	solid SS
B	15	90	blunt (electroerosion)	solid RTV, thin-skin Invar	solid SS
C	10, 15, 20	90	sharp	solid RTV	solid Plexiglas
D	10, 15, 20	90	blunt (handmade)	solid RTV	solid Plexiglas
E	15	30, 90	sharp	solid RTV, thin-skin Invar	solid Plexiglas
F	15	30, 90	sinusoidal (sharp)	solid RTV, thin-skin Invar	solid Plexiglas

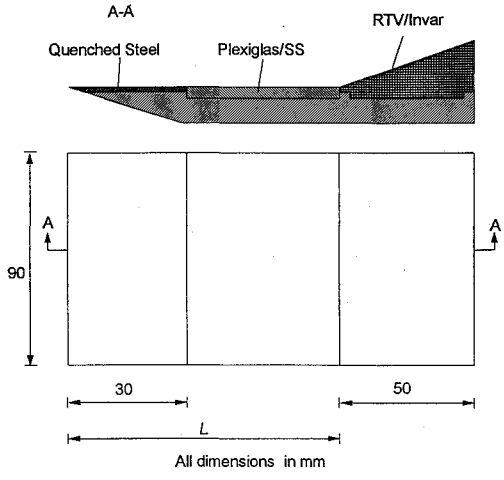

Fig. 1 Model layout.

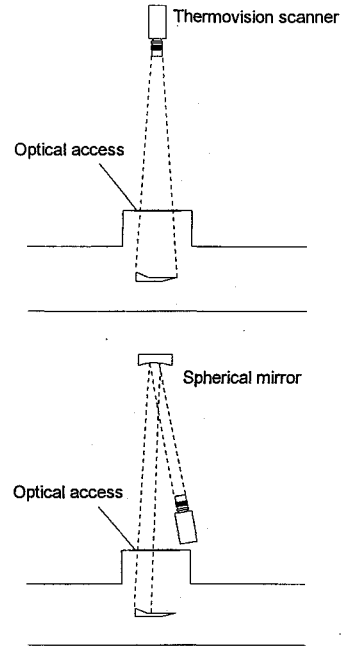

Fig. 2 IR imaging system optical configurations.

At the beginning of each test run, the model (which is initially in a remote position at room temperature) is vertically injected into the stream. The rise in time of its surface temperature is measured by viewing the model with an IR camera. A time sequence of thermograms is generally recorded during the test runs. Injection time is about 0.15 s and testing duration typically of 2 s.

Different types of models have been tested (see Table 1). They differ from each other in the leading-edge (LE) shape, the ramp angle value α, and the flat plate length L; the span for all of the models is 90 mm. Figure 1 illustrates the general configuration of the models. The ramp portion of the model is made of solid RTV 147 or thin-skin (0.2 mm thick) Invar®, whereas the LE is made of quenched steel with a 15-deg bevelled edge angle for all of the models. The flat plate segment is made of solid stainless steel (SS) for models A and B and solid Plexiglas® for models C, D, E, and F. The bluntness and the sinusoidal shape of the leading edge of the models B and F, respectively, has been obtained (and thus in some sense controlled) by means of an electroerosion process. For model D the bluntness has been achieved by hand. The sharp LE diameter of models A, C, and E is approximately 50 μm, whereas that of the round LE of model D is 300 μm; the LE diameter of model B is 500 μm. In order to investigate the dependence of the wavelength of heat transfer striations on the LE shape, and/or its nonuniformities, model F, with a sinusoidal LE, has been also tested. The wavelength of such a sinusoidal LE is 2 mm and the amplitude is 0.5 mm. End plates have been used with all of the models.

The reason for the use of RTV or Plexiglas is that, owing to the relatively low-thermal-diffusivity coefficient (2.31×10^{-7} and 1.09×10^{-7} m^2/s, respectively), the thermal sensitivity in detecting spanwise temperature fluctuations is enhanced. Moreover, the thermal penetration depth is very small and the thin-film sensor model (semi-infinite wall) can be used to correlate the measured wall temperature to the heat transfer coefficient.

Where the measurement surface is made of Plexiglas, in order to enhance IR radiation detection it is necessary to coat it with a (thermally) black paint. On the other hand, the RTV surface emissivity coefficient is sufficiently high (the value measured by present authors in the IR wavelength range of measurement is about 0.93), so that the IR measurements can be carried out without any painting.

An AGEMA 900 IR system has been employed to obtain the data presented. The total field of view, which depends on the employed optics, is scanned by the Cd-Te-Hg detector (working in the 8–12 μm IR window) and a frame of 136 noninterlaced lines is produced in 1/15 s. Nominal sensitivity, expressed in terms of noise equivalent temperature difference, is 0.07°C when the scanned object is at ambient temperature. The scanner spatial resolution indicated by AGEMA is 230 instantaneous fields of view (IFOVs) per line at 50% slit response function (SRF). A/D conversion (12 bits) is performed within the camera itself. The computerized system allows the acquisition of a time sequence of thermal images. The system software for the acquisition and handling of the thermal image (which consists of a frame of 272 × 136 pixels) is the AGEMA ERIKA. All of the other details concerned with the viewing procedure may be found in Ref. 12.

Figure 2 depicts the two optical configurations employed during the tests. The upper system refers to the basic configuration for which a frame of 180×90 mm^2 (1.5 pixels/mm) is obtained at a viewing distance of 1 m. The configuration shown in the lower figure has been designed to obtain higher spatial resolution. In this case a spherical mirror (120 mm in diameter and having a focal length of 600 mm) has been employed in order to obtain a frame of 60×30 mm^2 (i.e., a spatial resolution of 4.5 pixels/mm).

Data Reduction

As already mentioned, because of the short measuring time the thermal penetration depth can be generally considered relatively small everywhere on the model surface; therefore, the one-dimensional semi-infinite wall thermal model can be considered. The present application constitutes an inverse heat conduction problem since the surface heat flux is determined (at every pixel location) from the measured temperature history on the surface of the heat conducting body.

It is well known that if the analysis is restricted to the semi-infinite solid, the net exchanged heat flux $q(t)$ at the instant t can be expressed as

$$q(t) = \sqrt{\frac{\rho c k}{\pi}}\left[\frac{\phi(t)}{\sqrt{t}} + \frac{1}{2}\int_0^t \frac{\phi(t) - \phi(\lambda)}{(t-\lambda)^{\frac{3}{2}}}\,d\lambda\right] \quad (1)$$

where $q(t) = q_c(t) - q_r(t)$ represents the difference between the convective heat flux and the radiative one. The symbol ϕ is the temperature difference $T_w(t) - T_{wi}$, where T_{wi} is the initial value of the wall temperature T_w; ρ, c, and k are the mass density, the specific heat, and the thermal conductivity coefficient of the model material, respectively. Usually the integral of Eq. (1) is evaluated numerically by using one of the algorithms accepted for aerospace application.[14]

Generally such algorithms are sensitive to temperature measurement errors, and one should be very cautious when using them with noisy data. Moreover, the approach based on Eq. (1) needs a relatively high-sampling rate and a good evaluation of the initial temperature T_{wi}. In the present case, due to the frame frequency of the IR camera (1/15 s), the first requirement is not fully satisfied; furthermore, T_{wi} is not very accurate because of the overheating experienced by the model when it crosses the turbulent boundary layer developing over the wind-tunnel walls.

An alternative approach that experience has shown to work better[15] is based on the assumption that the direct problem yields a certain time variation law (discussed subsequently) for the heat flux, in which some free parameters are present. Such parameters are then found so that the computed temperatures agree (to a certain accuracy level) with the experimentally measured temperatures. The extent of the fit or agreement is determined by the ordinary least squares criterion.

In the case of flow conditions invariant during a test, the convective heat transfer rate varies linearly with the wall temperature for a constant heat transfer coefficient h:

$$q_c = h(T_{\text{aw}} - T_w) \quad (2)$$

where T_{aw} is the flow adiabatic wall temperature.

The solution of the heat diffusion equation in solids based on the preceding boundary condition may be obtained by Laplace transform as

$$T_w = T_{wi} + (T_{\text{aw}} - T_{wi})\left[1 - e^{\beta^2}\text{erfc}(\beta)\right] \quad (3)$$

with

$$\beta = h\sqrt{t}/\sqrt{\rho c k} \qquad \text{and} \qquad \text{erfc}(\beta) = 1 - \text{erf}(\beta)$$

In the presence of the radiative heat flux, under the assumption that the convective and radiative contributions are uncoupled, Eq. (3) may be modified to take into account the radiative correction,

$$T_w = T_{wi} + (T_{\text{aw}} - T_{wi})\left(1 - e^{\beta^2}\text{erfc}(\beta)\right) - (q_r/h) \quad (4)$$

where $q_r = \sigma\varepsilon(T_w^4 - T_{\text{amb}}^4)$, where σ is the Stefan–Boltzmann constant, ε the emissivity coefficient, and T_{amb} the ambient temperature.

The adiabatic wall temperature T_{aw} is obtained via the recovery factor r: $T_{\text{aw}}/T_e = 1 + r(\gamma - 1)M_e^2/2$, where T_e and M_e are the stream temperature and Mach number outside the boundary layer and γ is the ratio of specific heats. The recovery factor r is taken equal to $Pr^{1/2}$ or $Pr^{1/3}$, where Pr is Prandtl number, depending on whether the flow is assumed laminar or turbulent.[16] Over the ramp T_e and M_e are evaluated from the oblique shock solution. In the present application the least squares method consists of finding h and T_{wi} in order to minimize the function

$$\sum_{j=1}^{n}(Y_j - T_{wj})^2 \quad (5)$$

where Y_j is the j term of the n experimentally measured temperature values and T_{wj} is the predicted one by means of Eq. (4), both of these being taken at time t_j and at the same location.

Hereafter the heat transfer data are reduced to a nondimensional form by introducing the Stanton number $St = h/(\rho_\infty c_{p\infty} V_\infty)$ where ρ_∞, $c_{p\infty}$, and V_∞ are the mass density, the specific heat at constant pressure, and the velocity of the freestream, respectively.

It is noted that in the present tests, because of the relatively high camera spatial resolution, as well as low heat transfer oscillations wavelength, the need to apply an image restoration technique on acquired data is practically negligible. However, measured temperatures are corrected so as to take into account lateral conduction effects by using the temperature amplitude transfer function introduced by de Luca et al.[8]

An error analysis, based on IRIS calibration accuracy and repeatability of measurements, indicates that heat transfer coefficients measurements are accurate to within about ±8%. This estimate reflects also the contribution of flowfield nonuniformity.

Results

The streamwise Stanton number distributions over the flat plate/ramp configuration of model C are shown in Fig. 3 for the flap angle $\alpha = 10$ deg and three different unit Reynolds numbers Re_u. Note that the results of model C, having the flat plate segment made of Plexiglas and thus particularly suitable for IR measurements, will be the focus of discussion. For the model under consideration the hinge line is located at the streamwise distance $x = 90$ mm from the leading edge. The sudden decrease of the heat transfer coefficient upstream of the ramp recovers the laminar nature of the viscous separation region.[17,18] Note also that the Stanton number distributions over the ramp do not show any peak suggesting that under the present conditions reattachment is probably transitional. Near the hinge line the curves are quite irregular because at the corner the semi-infinite thermal model is invalid. In order to assess the accuracy of the present measurements, in Fig. 3 the streamwise Stanton number trends are compared with the theoretical solution of the laminar hypersonic boundary layer over a flat plate obtained by using Eckert's[19] reference temperature method. The corresponding curves agree to within less than 10%, and this finding confirms the presence of laminar boundary-layer development.

Analogous streamwise Stanton number trends for model F (with flat plate length $L = 90$ mm) having the sinusoidal leading edge are depicted in Fig. 4. In this case the minimum pocket of the heat

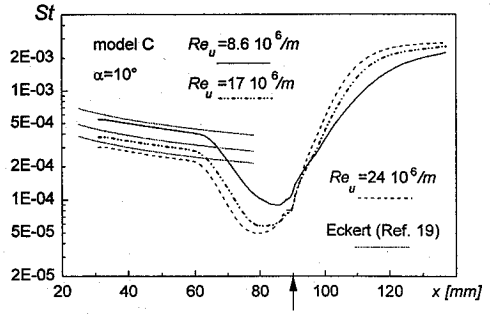

Fig. 3 Streamwise distributions of average Stanton number for three unit Reynolds numbers over model C (arrow indicates the hinge line position).

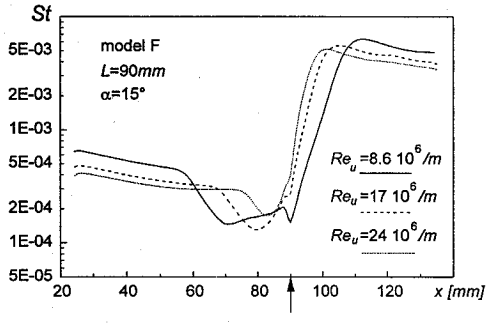

Fig. 4 Streamwise distributions of average Stanton number for three unit Reynolds numbers over model F (arrow indicates the hinge line position).

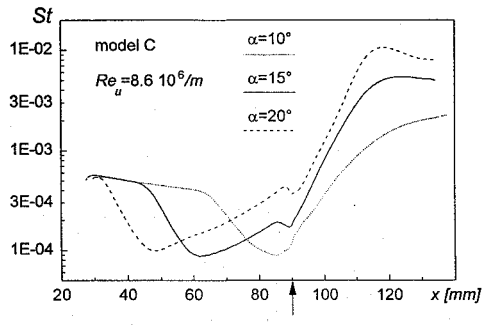

Fig. 5 Streamwise distributions of average Stanton number for three ramp angles over model C (arrow indicates the hinge line position).

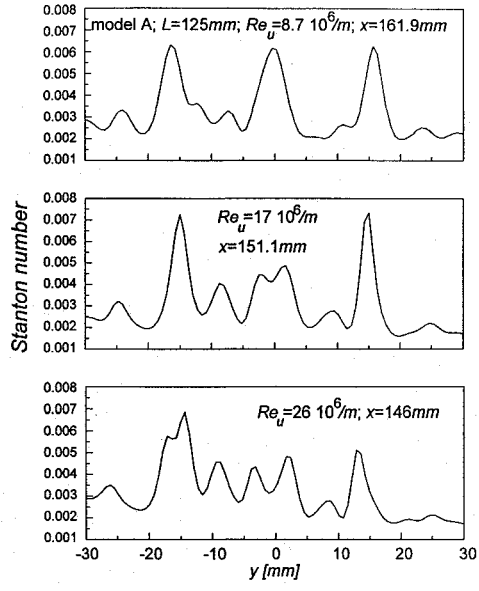

Fig. 6 Stanton number spanwise distributions near the reattachment for three unit Reynolds numbers over model A.

transfer coefficient reduces in size with increasing unit Reynolds number, and a peak is clearly evident over the ramp, whose level diminishes as the Reynolds number increases. This situation is ascribed to the occurrence of a transitional or turbulent separation and a subsequent turbulent reattachment.[17] It is generally recognized that the peak heat flux occurs at a small distance downstream of the reattachment point.[20]

The Stanton number variations measured over model C for flap angles α of 10, 15, and 20 deg and $Re_u = 8.6 \times 10^6$/m are shown in Fig. 5. The effect linked to the increase of the flap angle is that of moving the location of the (laminar) separation upstream. The Stanton number over the ramp attains its highest values at the highest ramp angle of 20 deg (due to the stronger interaction). For this last situation the very clear Stanton number peak denotes the presence of a turbulent reattachment. Note that the Stanton number distributions over the ramp reported up to now refer to spanwise average values since in all of the tested flow conditions the heat transfer coefficient exhibits a spanwise periodic variation that following Inger's reasoning[1] could be due to the formation of Goertler type vortices developing in the reattaching flow region. It will be seen later, however, that the onset of such three-dimensional variations is strongly related to the leading-edge shape and/or its nonuniformities.

To demonstrate this effect, the spanwise Stanton number trends over the ramp of model A with $L = 125$ mm for the three tested Reynolds numbers are shown in Fig. 6. Such distributions are taken along the spanwise y direction where the aerodynamic heating is very close to its maximum value (as usual, x is measured from the model LE). Relatively high Reynolds number as well as flap angle values (not shown here) seem to have the effect of reducing the wavelength of heat transfer oscillations. As far as the amplitude of such fluctuations is concerned, it seems that its value remains practically constant (about 30% of the average value).

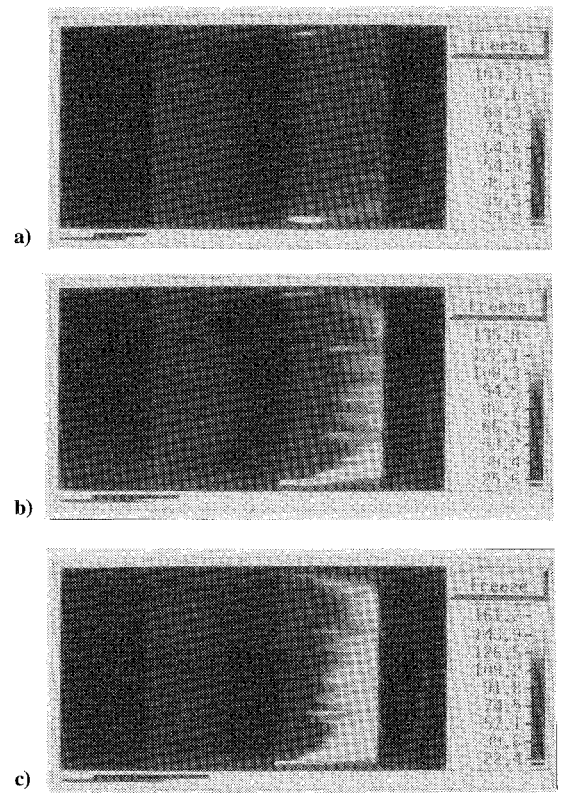

Fig. 7 Thermograms of model C for $\alpha = 10$ deg and three unit Reynolds numbers: a) $Re_u = 8.6 \times 10^6$/m, b) $Re_u = 17 \times 10^6$/m, and c) $Re_u = 24 \times 10^6$/m.

These considerations may be recovered by examining the thermograms taken over model C, $\alpha = 10$ deg, shown in Fig. 7. Each thermogram represents the thermal map (the flow comes from the left side) recorded at a certain instant during the test. In the present case, the sixth image of the sequence, acquired about 0.2 s from the instant when the model is in position, is utilized. Two straight vertical lines are clearly visible on the thermograms. One, on the left side of the figure, separates the cold (black) stainless-steel leading-edge region from the warmer (gray) Plexiglas part; the other, on the thermogram right side, represents the edge of the hot (clear) ramp. The hinge line is located approximately in correspondence to the vertical color change line between the cold (black) flat plate region, where the flow is separated, and the beginning of the ramp. On the ramp, temperature rapidly increases and attains a maximum. The presence of the temperature (and so heat transfer) striations over the ramp is clearly visible. Besides providing a flowfield visualization record, the sequence of thermograms of Fig. 7 yields a typical example of the potential of IR technique. In fact, whereas other more conventional or standard techniques used to visualize the surface flow (e.g., oil films and thermosensitive paints) need the model to be properly treated before each test run, IRIS does not require any preparation (the black coating, if necessary, is needed just at the beginning of the entire tests session).

The effect of the flat plate length L on the peak Stanton number does not seem very important. Such an effect has been investigated by using model A (with $\alpha = 15$ deg). The spanwise Stanton number distributions close to the reattachment line are shown in Fig. 8 for $L = 40$, 90, and 125 mm and $Re_u = 8.7 \times 10^6$/m. In other words, here the results refer to different Reynolds numbers Re_L based on the flat plate length. As the most significant result, it is evident that the wavelength of heat transfer periodic variations decreases as a function of Reynolds number based on flat plate length.

A basic question, namely, what induces the spanwise Stanton number striations over the ramp, deserves more attention. As mentioned in the introduction, Inger[1] attributed them to a centrifugal (Goertler) instability of the boundary layer over the concave dividing streamline forming in the presence of the separated flow due to the strong viscous interaction. It has to be pointed out, however,

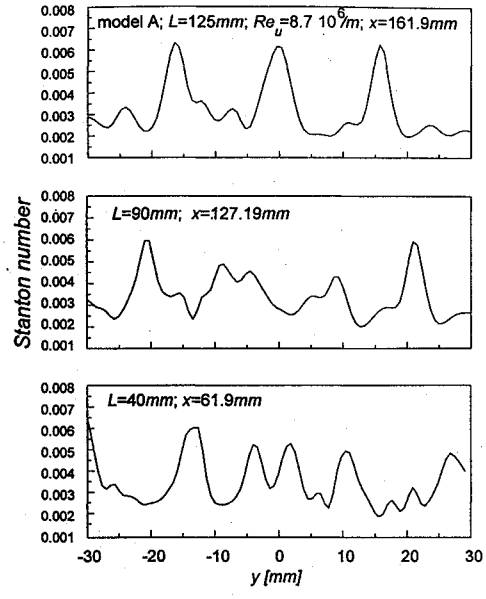

Fig. 8 Stanton number spanwise distributions near the reattachment for three flat plate lengths over model A.

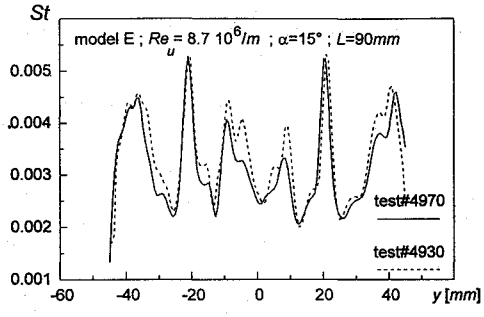

Fig. 9 Repeatability of heat transfer oscillations over the same model E.

that a practically deterministic influence of the LE geometry on the wavelength of oscillations has been observed. To illustrate this influence, a comparison between two spanwise Stanton number variations (over model E, flap angle of 15 deg, $Re_u = 8.7 \times 10^6$/m, $L = 90$ mm) recorded along the same spanwise line is shown in Fig. 9. Measurements have been taken during two tests repeated after a significantly long time, so as to include also the effects due to the imprecise setting of stagnation temperature and pressure, model attitude, etc. The almost perfect superimposition of the two recordings is clearly evident. On the contrary, it has been found (not shown) that two models macroscopically identical, having also the same LE radius of curvature but with microscopically different leading edges, lead to a quite different structure of the heat transfer periodic variations.

To further illustrate the nature of the heat flux striations, it was decided to build a model having regular and controlled LE nonuniformities, namely, model F with a sinusoidal LE. Model F has also two types of interchangeable ramp to compare IR and thermocouples measurements. In Fig. 10 the spanwise Stanton number variations recorded over both the ramps ($L = 30$ mm) at the streamwise location $x = 44$ mm (as measured from the LE) show a nearly periodic trend with an average wavelength practically equal to that of the leading edge (2 mm). Note that the Invar thin-skin ramp has been equipped with a traversing mechanism to allow the ramp itself to be moved in the spanwise direction.[21] In fact, it has been impossible to put on the ramp as many thermocouples as the problem needed to obtain an adequate spanwise spatial resolution. Thus, an alternative approach consists of moving the thermocouples by moving the ramp from run to run. The position of temperature striations has been observed to remain unchanged for several subsequent tests (on the very same leading edge) when the ramp was moved laterally. IR and thermocouples curves agree very well. In this case, due to the small wavelength, lateral conduction corrections are quite important.

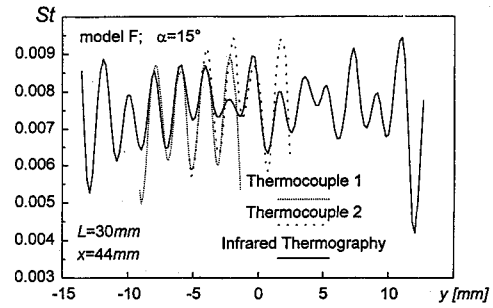

Fig. 10 Comparison between IR thermography and thermocouples data for sinusoidal LE model F.

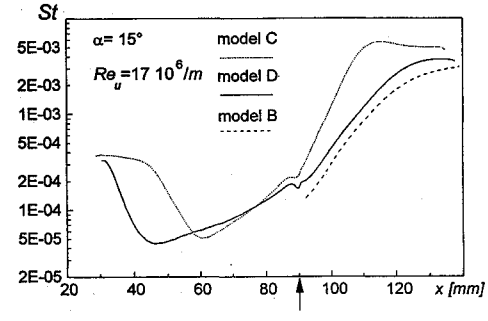

Fig. 11 Influence of leading-edge bluntness on Stanton number streamwise distribution (arrow indicates the hinge line position).

Summarizing the results of Figs. 9 and 10 one may conclude that the leading edge plays a key role in the selection mechanism of the most amplified wavelength of disturbances (i.e., the nature of striations).

The influence of the LE bluntness may be analyzed by looking at the streamwise Stanton number distributions taken for $\alpha = 15$ deg and $Re_u = 17 \times 10^6$/m over models C, B, and D (Fig. 11) having sharp and blunt leading edges, respectively. Whereas the heat transfer over the flap at the reattachment decreases with increasing the leading-edge bluntness, the (laminar) separation point before the hinge line moves strongly upstream when the LE is rounded. This effect is in qualitative agreement with full Navier–Stokes computations[20] but seems to be opposite to that found by Coet.[17] However, one has to consider that in the present tests the blunt leading edge is simply of thicker sharp type, whereas the model used by Coet[17] had a real round LE, the curvature radius of which ranged from 2.5 to 5 mm. Note that data relative to model B are taken on the ramp only, because of the fact that the flat plate was made of solid stainless steel and the semi-infinite wall does not apply. It should also be pointed out that the different flat plate materials used for models B and D do not significantly influence the boundary-layer development (and, consequently, the heat transfer level) because of the relatively low temperature difference (about 10°C) attained on the two flat plates. The effect of the bluntness over the oscillations wavelength is not reported since it is not very clear.

The results relative to the peak heat flux can be represented using either Hung and Barnett's[22] correlation or that proposed by Simeonides et al.[18] According to the Simeonides et al. correlation,[18] which in general may be written for fully laminar or fully turbulent peak heatings and laminar or turbulent reference levels, in the present paper (average) peak heat flux data are reduced by defining a function $F(Re_{L\mathrm{pk}})$, where $Re_{L\mathrm{pk}}$ is the Reynolds number based on the distance L_{pk} between the leading edge and the streamwise location of the heat flux peak,

$$F = \frac{q_{\mathrm{pk}}/q_{\mathrm{fp}}}{(L_{\mathrm{pk}}/\bar{L}_{\mathrm{pk}})^n (p_{\mathrm{pk}} V_{\mathrm{pk}}/p_{\mathrm{fp}} V_{\mathrm{fp}})^{1-n}} \tag{6}$$

where q_{pk} is the (average) peak value of the heat flux, q_{fp} is the flat plate laminar heat flux corresponding to the Reynolds number $Re_{L\mathrm{pk}}$. Also, $\bar{L}_{\mathrm{pk}}$ is the streamwise distance between the reattachment point and the heat flux peak, p is pressure, V is velocity, and $n = 0.2$ (which is the value proposed in Ref. 18 for turbulent peak heating). Following Alziary de Roquefort,[20] the inviscid value for $p_{\mathrm{pk}} V_{\mathrm{pk}}/p_{\mathrm{fp}} V_{\mathrm{fp}}$ has been used and the location of the reattachment

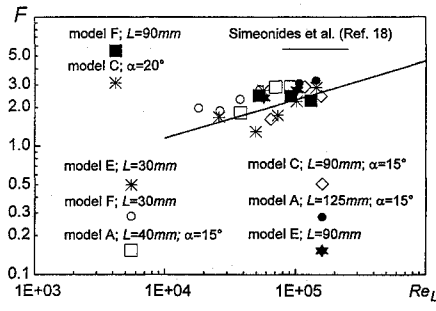

Fig. 12 Correlation of average peak heat flux data.

point has been estimated as the location of the inflexion point on the streamwise distribution of the Stanton number averaged in the spanwise direction. Results, presented in Fig. 12, fit the Simeonides correlation,[18] $F = 0.072(Re_{L\mathrm{pk}})^{0.3}$ (full line), within a ±20% band for fully turbulent peak heating data. A greater spread is observed for transitional reattachments data, i.e., at about $Re_{L\mathrm{pk}} < 6 \times 10^4$. One should, however, stress that the results are sensitive to the estimation of $\bar{L}_{\mathrm{pk}}$.

Conclusions

An experimental investigation has been carried out to analyze some aspects of shock/boundary-layer interaction in nominally two-dimensional hypersonic wedge flow, namely, over flat plate/ramp configurations. These flow conditions are two dimensional only geometrically because some spanwise periodic variations (striations) of the heat flux over the ramp in the reattaching flow region have been observed. The measurements, made by means of a computerized IR imaging system, have been performed in a blowdown wind tunnel at Mach number equal to 7.14 for different unit Reynolds numbers. The ramp, following the flat part of the models, is made of RTV, low-thermal-conductivity material that allows a better visualization of the heat transfer fluctuations. The influence of the leading-edge shape, flat plate length, and ramp angle on the separation region, average heat transfer at reattachment, and wavelength of the heat transfer oscillations has been analyzed and the most significant results may be summarized as follows.

Regarding unit Reynolds number, whereas for transitional reattachments the heat flux level over the ramp does not show any peak, for fully turbulent reattachments the peak heat flux diminishes as the unit Reynolds number increases. The wavelength of the spanwise variations decreases with increasing unit Reynolds number.

For ramp angle, the separation region before the hinge line moves upstream with increasing the ramp angle; the Stanton number average level on the ramp increases accordingly, while the spanwise oscillation wavelength decreases.

Regarding flat plate length, the influence of L on the peak Stanton number does not seem very important; when, as in the present tests, L is varied by keeping unit Reynolds number constant; it is found that shorter wavelengths of oscillations correspond to lower Reynolds number based on flat plate length.

The leading-edge geometry plays a key role in the mechanism of selection of the wavelength of the heat flux oscillations observed over the ramp. In fact, a practically deterministic influence of the leading-edge geometry over the wavelength has been found experimentally, which may be summarized in two basic results: repeatability of the oscillations under the same test conditions and periodic variations wavelength equal to that of the sinusoidal LE.

For leading-edge bluntness, within the present tests the finding is that a blunt leading edge moves the separation region upstream, whereas the Stanton number average value on the ramp diminishes.

The influence of the parameters under study on the amount of the amplitude of the oscillations is not very clear. As a general result, it is found that such an amplitude may rise up to about 35% with respect to the spanwise average value. Data relative to the average peak heat flux agree well with the semiempirical correlation proposed by Simeonides.

As a final comment, the present authors wish to emphasize that this paper is basically restricted to the presentation of experimental findings showing three-dimensional effects in hypersonic compression ramp flows. Whether and how the spanwise periodic variations of the heat transfer coefficient can be related to the development of Goertler type vortices seems to be still unknown. Therefore, further experimental works and theoretical studies are strongly needed.

Acknowledgments

This work has been supported by Dassault Aviation within the Hermes research and development space program. It has been also supported partially by the Galileo program.

References

[1]Inger, G. R., "Three-Dimensional Heat- and Mass-Transfer Effects Across High-Speed Reattaching Flows," *AIAA Journal*, Vol. 15, No. 3, 1977, pp. 383–389.

[2]Coet, M. C., "Etude expérimentale des effets de la création d'une couche d'entropie sur l'interaction onde de choc-couche limite en écoulement hypersonique," ONERA R.T. 16/4362 AY, Chatillon sous Bagneux, France, July 1991.

[3]Aymer de la Chevalerie, D., and Fonteneau, A., "Goertler Vortices in Hypersonic Flows: the Ramp Problem," Final Rept. 1993, Laboratoire d'Etudes Aérodynamiques, URA C.N.R.S. 191, Poitiers, France, 1993.

[4]Simeonides, G., "Hypersonic Shock Wave Boundary Layer Interactions over Compression Corners," Ph.D. Thesis, Von Kármán Inst./Univ. of Bristol, Dept. of Aerospace Engineering, Bristol, UK, April 1992.

[5]El-Hady, N., and Verma, A. K., "Growth of Goertler Vortices in Compressible Boundary Layers along Curved Surfaces," *Journal of Engineering and Applied Sciences*, Vol. 2, 1983, pp. 213–238.

[6]Spall, R. E., and Malik, M. R., "Goertler Vortices in Supersonic and Hypersonic Boundary Layers," *Physics of Fluids A*, Vol. 1, No. 11, 1989, pp. 1822–1835.

[7]Jallade, S., "Etude theorique et numerique de l'instabilité de Goertler," Ph.D. Thesis, Institut National Polytechnique de Toulouse, Toulouse, France, Jan. 1990.

[8]de Luca, L., Cardone, G., Aymer de la Chevalerie, D., and Fonteneau, A., "Goertler Instability of Hypersonic Boundary Layer," *Experiments in Fluids*, Vol. 16, 1992, pp. 10–16.

[9]Rudy, D. H., Thomas, J. L., Kumar, A., Gnoffo, P. A., and Chakravarthy, S. R., *AIAA Journal*, Vol. 29, No. 7, 1991, pp. 1108–1113.

[10]Carlomagno, G. M., de Luca, L., and Alziary de Roquefort, T., "Mapping and Measurements of Aerodynamic Heating and Surface Flow Visualization by Means of IR Thermography," *Multiphase Flow and Heat Transfer*, edited by X. J. Chen, T. N. Veziroglu, and C. L. Tien, Vol. 2, Hemisphere, New York, 1991, pp. 1316–1324.

[11]Balageas, D. L., Boscher, D., Deom, A., Fournier, J., and Gardette, G., "Measurement of Convective Heat Transfer Coefficients in Wind Tunnels Using Passive and Active Infrared Thermography," *La Recherche Aerospatiale*, Vol. 4, 1991, pp. 51–72.

[12]de Luca, L., Cardone, G., Carlomagno, G. M., Aymer de la Chevalerie, D., and Alziary de Roquefort, T., "Flow Visualization and Heat Transfer Measurements in Hypersonic Wind Tunnel," *Experimental Heat Transfer*, Vol. 5, 1992, pp. 65–78.

[13]Gartenberg, E., and Roberts, A. S., Jr., "Twenty-Five Years of Aerodynamic Research with IR Imaging," *Journal of Aircraft*, Vol. 29, No. 2, 1992, pp. 161–171.

[14]Cook, W. J., and Felderman, E. J., "Reduction of Data from Thin Film Heat Transfer Gages: A Concise Numerical Technique," *AIAA Journal*, Vol. 4, No. 3, 1966, pp. 561, 562.

[15]Beck, J. V., Blackwell, B., and St. Clair, C. R., Jr., *Inverse Heat Conduction*, Wiley, New York, 1985.

[16]Shapiro, A. H., *The Dynamics and Thermodynamics of Compressible Fluid Flow*, Vol. 2, Ronald Press, New York, 1954.

[17]Coet, M. C., "Etude expérimentale de l'effet d'une couche d'entropie sur l'interaction onde de choc/couche limite en écoulement hypersonique," ONERA R.T. 29/4362 AY, Chatillon sous Bagneux, France, Dec. 1992.

[18]Simeonides, G., Haase, W., and Manna, M., "Experimental, Analytical, and Computational Methods Applied to Hypersonic Compression Ramp Flows," *AIAA Journal*, Vol. 32, No. 2, 1994, pp. 301–310.

[19]Eckert, E. R. G., "Engineering Relations of Friction and Heat Transfer to Surfaces in High Velocity Flow," *Journal of Aerospace Sciences*, Vol. 22, No. 8, 1955, pp. 585–587.

[20]Alziary de Roquefort, T., "Progress in Low Enthalpy Hypersonic Wind Tunnel Testing," *Proceedings of the 2nd European Symposium on Aerothermodynamics for Space Vehicles*, European Space Agency, ESA SP-367, Paris, 1995, pp. 575–582.

[21]Aymer de la Chevalerie, D., Fonteneau, A., de Luca, L., and Cardone, G., "Goertler Vortices in Hypersonic Flow: The Ramp Problem," *Experimental Thermal and Fluid Science* (submitted for publication).

[22]Hung, F. T., and Barnett, D. O., "Shock Wave-Boundary Layer Interference Heating Analysis," AIAA Paper 73-237, Jan. 1973.